HHS Public Access

Author manuscript

Hear Res. Author manuscript; available in PMC 2020 December 01.

Published in final edited form as:

Hear Res. 2019 December ; 384: 107813. doi:10.1016/j.heares.2019.107813.

Recovery from Tympanic Membrane Perforation: Effects on Membrane Thickness, Auditory Thresholds, and Middle Ear Transmission

Lingling Cai[1,2], **Glenna Stomackin**[1], **Nicholas M. Perez**[1,4], **Xiaohui Lin**[1], **Timothy T Jung**[1,3], **Wei Dong**[1,3]

[1]VA Loma Linda Healthcare System, Loma Linda, CA, 92357

[2]Department of Radiology, the Ninth People's Hospital Affiliated to Shanghai Jiaotong University, School of Medicine, China

[3]Department of Otolaryngology – Head and Neck Surgery, Loma Linda University Health, Loma Linda, CA 92350

[4]School of Computer Science and Engineering, California State University San Bernardino, San Bernardino, CA 92407

Abstract

Sounds delivered to the ear move the tympanic membrane (TM), which drives the middle-ear (ME) ossicles and transfers the acoustic energy to the cochlea. Perforations of the TM result in hearing loss because of less efficient sound conduction through the ME. The patterns of TM motions, and thus ME sound transmission, vary with frequency and depend on many factors, including its thickness. In this study, we measured TM thickness, auditory brainstem responses (ABR) and ME transmission immediately following a controlled pars tensa perforation and after 4 weeks of spontaneous recovery in a gerbil model. It is found that after recovery, the hearing thresholds showed a sloping pattern across frequencies: almost back to normal level at frequencies between 2 to 8 kHz, sloping loss in the low (< 2 kHz) and mid-frequency (8–30 kHz) range, and little restoration at frequencies above 30 kHz. This pattern was confirmed by the measured ME pressure gains. The thickness of the healed TM did not return to normal but was 2–3 times larger over a significant portion of the membrane. The increased thickness was not limited to the perforated area but expanded into intact regions adjacent to the perforation, which led to an increased thickness in general. Combined, these results suggest that TM thickness is an important factor in determining its vibration patterns and efficiency to transfer sounds to the ossicles and thus influencing ME sound transmission, especially for high-frequency sounds. The results provided both structural and functional observations to explain the conductive hearing loss seen in

Corresponding author: Wei Dong, VA Loma Linda Healthcare System, 11201 Benton Street, Loma Linda, CA, 92357, Tel.: 909 825 7084 Ext. 2899, Fax: 909 796 4508, Wei.dong@va.gov; wdong@llu.edu.

patients with abnormal TMs, e.g., caused by otitis media, spontaneously healed post-perforation or repaired via tympanoplasty, in the clinic.

Keywords

hearing; middle-ear sound transmission; optical coherence tomography; tympanic-membrane thickness; healed tympanic-membrane post-perforation; middle-ear pressure gain

1. INTRODUCTION

The tympanic membrane (TM) has a unique set of properties, such as its elasticity, thickness, and shape that determine how it vibrates in response to sounds. As the TM vibrates, this motion is transmitted to the malleus that attaches to it, forming the initial drive to the ossicular chain. Across frequencies, TM moves in a frequency-dependent manner. At low frequencies the whole TM moves in phase with the stimulus. For higher frequencies, the vibration pattern becomes more complex with different TM areas moving in different phases (Cheng et al., 2013; Cheng et al., 2010; Khanna et al., 1972; Rosowski et al., 2009). The TM thickness is an important factor in setting these vibration patterns as it directly determines both the elasticity and stiffness of the membrane, and thus impacts sound transmission. Detailed mapping of TM thickness distribution is thus important for a more comprehensive understanding of the sound transmission under normal and pathological conditions as it may explain TM related conductive hearing loss (CHL) in the clinic, and help the development of theoretical models of middle ear (ME) dynamics. However, only limited data exists on TM thickness distribution, especially under abnormal conditions.

The thickness of human TM has been measured using conventional methods such as optical or electron microscopy with the thickness measured over a limited extend (30–150 μm) of the membrane [e.g., (Decraemer et al., 2008; Lim, 1970)]. Recently, optical coherence tomography (OCT) has been used for mapping the distribution of TM thickness. This is a technique that can obtain noninvasive, cross-sectional images from biological tissues using low-coherence interferometry (Huang et al., 1991). It is analogous to ultrasound imaging, except that it uses light rather than sound. The ability of OCT to provide high-resolution images over a depth of a few millimeters makes it attractive for TM imaging (Ramier et al., 2018), and several recent studies have used OCT to visualize the TM and the ME structures behind the TM (Djalilian et al., 2008; Monroy et al., 2015; Nguyen et al., 2012; Pitris et al., 2001; Shelton et al., 2014; Tan et al., 2018). It has also been used to measure the TM thickness in living humans, yielding estimates between 50–120 μm across the membrane (Hubler et al., 2015; Van der Jeught et al., 2013). The results obtained by the different methods are similar, and confirm that the OCT technique could be used for high-resolution, real-time imaging of TM and ME structures in the clinic.

Gerbils have been widely used in hearing research because they have similar hearing sensitivity/pattern at low frequencies as humans (Ryan, 1976), in contrast to many commonly used laboratory animals (Heffner et al., 2007). However, the reported normal TM thicknesses in gerbils were different across different studies. Von Unge et al. (von Unge et al., 1991) reported the gerbil pars tensa to be 3–5 μm in the central area and 20 μm near the

edges, while Teoh et al. (Teoh et al., 1997) found the mean pars tensa thickness to be ~19 μm. It is estimated that conventional histological techniques, such as tissue fixation and paraffin embedded tissue sectioning, can cause ~20–30% decrease in thickness in the central pars tensa region (Kuypers et al., 2005a). Without using conventional histological preparation, Kuypers et al. (Kuypers et al., 2005b) found the gerbil pars tensa to be ~6–14 μm, with a mean value of 28 μm along the annular edge.

TM perforations lead to CHL due to reductions of the effective drive to the attached ossicle (Stomackin et al., 2018; Voss et al., 2001). For a moderately sized perforation the TM heals spontaneously. However, elevated hearing thresholds remain because of the thicker and denser healed membrane (Cho et al., 2013; Garth, 1994). Several studies have explored the thickness of the healed TMs in animals. Rahman et al. (Rahman et al., 2005) reported that the healed area of the pars tensa in rat was about 25 μm thick at two weeks post-perforation, which equaled a fivefold increase compared to normal TMs. Stenfors et al. (Stenfors et al., 1980) performed a similar study in both cats and rats, and found that even 10-weeks post-perforation the healed perforation area was clearly thicker and did not exhibit a regular structure.

In the current study hearing and ME sound transmission was evaluated immediately after and following a one-month recovery from a 50% perforation of pars tensa in the gerbil ear by measuring auditory brainstem responses (ABR) and ME pressure gains (MEPG). We also obtained cross-sectional TM images across the entirety of the membrane using OCT from which we reconstructed TM thickness maps. We found that the perforation in the TM had closed after four weeks of spontaneous recovery, but that the membrane was much thicker (2–3×) compared to pre-perforation. Functionally, both the ABR thresholds and MEPG returned to almost normal for frequencies between 2 to 8 kHz, while responses to low and mid-frequency stimuli (< 2 kHz and 8–30 kHz) only partially recovered. At the highest frequencies (>30 kHz), no signs of recovery were seen at all. These results indicate that TM thickness is an important factor for the coupling of ear-canal sounds to the inner ear, especially for high-frequency sounds. The current study correlates TM thickness and ME sound transmission in ears with normal or healed TMs, which helps to understand the mechanism underlying CHL in patients with healed or reconstructed TM via tympanoplasty, and can be used to formulate and/or validate models of the ME dynamics.

2. METHODS

To establish the relationship between TM thickness and ME function, experiments were performed to assess the effects of a spontaneously healed TM perforation on ME transmission. The left TM of young adult Mongolian gerbils were mechanically perforated by ~50% removal of the pars tensa [(Fig. 1A) and see related details in (Stomackin et al., 2018)], leaving pars flaccida and the ossicular chain intact. Throughout the text, we refer to this perforation as “TM perforation”. The right ears served as controls. The TM perforation was allowed to spontaneously recover for 4 weeks with weekly checks of healing and hearing using otoscopy and pure-tone induced ABR thresholds, respectively. Only animals that remained free of infection and wax build up in the ear canal over the whole recovery timeline were included in the statistical analysis. After the recovery period, ME sound

transmission was measured by *in vivo* recordings of MEPG (see Methods 2.2). Following the data acquisition, animals were euthanized and both TMs were immediately harvested and scanned under fresh, and later fixed, conditions using an OCT system to obtain its thickness (see Methods 2.3). The latter condition was included to allow a direct comparison of our results to previous observations that used histological preparations of the TM.

The care and use of animals were approved by the Institutional Animal Care and Use Committee (IACUC) of the VA Loma Linda Healthcare System. Twenty young adult Mongolian gerbils housed in autoclaved cages were used for this study, with 11 animals contributed to the post-50%-perforation testing. The other nine animals were used to finalize the experimental approach and explore the spontaneous healing process with different sizes of TM perforations (Stomackin et al., 2018).

2. 1 Tympanic Membrane Perforation and Monitoring over Healing Process

Animal anesthetics: Animals were anesthetized by an initial dose of a ketamine (80 mg/kg)/xylazine (10 mg/kg) cocktail i.p., with maintenance doses given as needed. While anesthetized, temperature was maintained at ~37° using a rectal probe attached to a Harvard Apparatus heating pad. After the initial TM perforation, as well as following the weekly healing checkups and ABR recordings, an anesthetic reversal dose of 0.2–1 mg/kg atipamezole was given.

Tympanic membrane perforation: Before perforating the TM, the animal's left ear canal was flushed with a 2% chlorhexidine solution, followed by sterile saline to clean. Then, the inferior portion of pars tensa was removed with a sterile 30-gauge needle attached to a sterile syringe using the manubrium and umbo as reference points (Fig. 1A). Pars tensa and perforation area were measured using the OCT system and imageJ to confirm that perforation size was ~50% [see also (Stomackin et al., 2018)]. Great care was taken to use only the minimum amount of force necessary to create the desired perforation, while keeping the ossicular chain intact. After recovering from the anesthetic, animals were brought back to autoclaved cages to minimize the chance of infection.

Healing checkups: Over the 4-week recovery time course, the animals were brought back weekly and anesthetized as described above for otoscopic evaluation and hearing tests. The healing process was visually monitored using a Stryker video-picture endoscope device attached to a Karl Storz 0-degree Hopkins 1218 scope, with which the pictures of the recovering pars tensa were taken. These pictures helped to determine if there were any other adverse side effects caused by TM perforation, such as wax build up or infection [see images in (Dong et al., 2019)]. Once the perforation had completely sealed, the animal's ear canal was flushed weekly with 1–2 drops of 0.2% salicylic acid solution (Epi-Otic), followed by warm sterile saline, to prevent excess wax build up and/or to remove any existing wax in the ear canal. Gerbils that developed ear infections or heavy wax build up at any point during recovery were removed from the study.

Auditory brainstem response (ABR) thresholds: ABR thresholds were determined immediately pre- and post-perforation, and weekly during the 4-week recovery period for

the left ear. ABR threshold measurements of the right (control) ears contributed to hearing evaluation under normal conditions.

A detailed description of the ABR recording system is given in an earlier study (Dong et al., 2019). Briefly, ABRs evoked by single tone bursts were recorded at 10 frequencies of 0.5, 2, 4, 5.6, 8, 11.3, 16, 22.6, 32, and 45 kHz, at sound pressure levels (SPL) of 0 to 80 dB SPL in 5 dB steps. To release any ME pressure that may build up during the recordings, the gerbil's pars flaccida was punctured using a sterile 100-μm pin before taking ABR measurements. This tiny hole is known to only influence hearing at very low frequencies (de La Rochefoucauld et al., 2010; Dong et al., 2013) and resealed in two days. Recording electrodes were placed under the skin with the active electrode positioned at the ipsilateral vertex of the skull, the reference electrode placed under the ear canal opening near the bulla location, and a ground electrode placed in the left rear leg. ABR thresholds were determined from the recordings by visually examining the ABR wave-I to determine the lowest sound level at which reproducible waveforms were observed.

2.2 Direct Measurements of Middle Ear Pressure Gain

After four weeks of recovery, experiments were performed to directly measure the sound evoked pressures close to the TM (P_{TM}) and in scala vestibuli (SV) near the stapes (P_{SV}) using a data acquisition system described in detail elsewhere (Dong et al., 2006; Dong et al., 2019; Stomackin et al., 2018). Middle ear pressure gain is defined (Dong et al., 2006; Stomackin et al., 2019) as the absolute ratio between the SV pressure near the stapes and pressure close to the TM: $MEPG=|P_{SV}/P_{TM}|$. The sound transmission time through the ME was evaluated by the MEPG phase group delay, defined as $\tau = -\Delta\Phi/\Delta f$, where $\Phi = \Phi_{PSV} - \Phi_{PTM}$, and f stands for the frequency.

Each animal was deeply anesthetized as described above. For the surgical preparation, the animal's skull was secured using dental cement (Durelon) to a head holder. The left pinna was removed and the ispilateral bulla was widely opened. A small hole (~200 μm) was created in the bony wall of the SV adjacent to the stapes for intracochlear pressure measurements (Dong et al., 2006). A micro pressure sensor (~125 μm OD) (Olson et al., 2015) was introduced into SV via this hole and positioned next to the stapes (Dong et al., 2006; Olson, 1998). The sensor was calibrated in air at both room and body temperature after construction and calibrated again before and after each experiment.

The sound system was coupled to the ear canal opening. It consisted of a Sokolich ultrasound microphone probe tube that passed through the center of a Y-shaped tube. Each arm of this tube was connected to a speaker (Fostex) using plastic tubing. The tip of the microphone was positioned within ~3 mm of the TM, and acoustic stimuli were calibrated at this point in decibels (dBs) re 20 $\mu Pa_{p\text{-}p}$. In this conficuration, the microphone noise level was ~10 dB SPL, with a 1-s data acquisition time. The non-perfect sealing of the sound system to the ear canal during the measurements influenced responses at frequencies below 1 kHz (de La Rochefoucauld et al., 2010).

Single-tone stimuli were generated by a commercial system [Tucker-Davis Technologies (TDT) System III] with a sampling rate of 200 kHz driving one Fostex speaker (Dong et al.,

2019; Stomackin et al., 2018). Stimulus generation, data acquisition, and analysis software was written in MATLAB and the TDT visual design studio. In the current study, high-level tones of 80 or 90 dB SPL were used to directly measure pressure responses at the ear canal and in the SV.

2.3 Tympanic Membrane Thickness Measurements Using Optical Coherence Tomography

Tympanic membrane preparations: After the MEPG measurements, animals were euthanized with Pentobarbital (390 mg/ml) and subsequently decapitated. Both the normal (right) and healed (left) TMs were harvested by separating the TM from connections to the bulla/cochlea, i.e., cutting the ME tendons and muscles and disarticulating incus and stapes. The tympanic ring supporting the TM cone-shape and attached manubrium were intact as shown in Fig. 1B. By doing this, the TM was preserved in its natural shape. The fresh specimens were scanned using the OCT system immediately after harvest, usually within 30 minutes after decapitation (referred to as “fresh condition”). After scanning, they were placed in a 4% formaldehyde fixative solution overnight. Fixed specimens were then scanned using the same OCT system after 24 hours of fixation (termed “fixed condition” in the text).

Thickness measurements using OCT: The OCT system (Thorlabs, TELESTO Series) and version 4.0 of the Thorlabs ThorImage OCT imaging software) allowed us to take quick 3D scans of the TM within 30 seconds (Fig. 1B). With this system it is not necessary to flatten the TM, its thickness can be determined across the entirety of its surface without compromising its natural 3D shape. The short scan time minimizes errors caused by tissue preparation and sectioning that were present when using conventional histological techniques. The refractive index was set to 1.44, as specified by Van der Jeught et al. (Van der Jeught et al., 2013). The tympanic ring of each TM was positioned to be as flat as possible to ensure perpendicular scanning. The umbo was chosen as the origin of a rectangular coordinate system and the specimen was oriented to have the x-axis perpendicular to the manubrium. Positive x- and y-coordinates are in the posterior and superior direction, respectively. The scanning pixel sizes used to ensure the entire TM fit within the 3D scanning zone were 4.71, 4.54, and 2.43 m along x-, y- and z-axis, respectively.

Once the 3D scan was completed, the cross-sections (slices) obtained by the “B-scan display” were used to measure the thickness of the TM at various points (Fig. 1C). A total of 11 slices were analyzed per TM, with one slice centered at the umbo, 5 slices positioned superior to the umbo, and 5 slices positioned inferior to the umbo, in ~0.3 mm increments (dotted lines in Fig. 1B and Fig. 1C). In each slice, and at approximately every 200 μm, we measured the thickness of the TM by manually drawing a line segment between its top and bottom surface. These line segments were perpendicular to these surfaces to account for non-horizontal orientations of the TM (see Fig 1C bottom panel) These thickness measurements (11 slices & 25–30/slice) were used to create the corresponding thickness maps using linear interpolation (MATLAB).

2.4 Statistical Analysis

Mean and standard deviation across samples or animals were calculated using MATLAB, i.e., TM thickness measured at similar locations and under similar conditions, hearing evaluations using ABR or MEPG were averaged at each testing frequency separately.

3. RESULTS

3.1 The Thickness of Normal Tympanic Membranes Under Fresh Condition

To determine the thickness of normal/non-perforated TM, the ears of nine gerbils were harvested following decapitation. Visually, these normal TMs appeared to be smooth and uniform, with all areas appearing to be relatively the same (Fig. 1B). Three representative cross-sectional OCT images (slices) of two of such normal, fresh TMs are shown in Figs. 1C and 2A. These slices correspond to ~1 mm superior to the umbo, at the umbo, and ~1 mm inferior to the umbo, which we refer to as slice 3, 0 and −4, respectively.

Figure 2B shows the corresponding thickness measurements at the three representative cross-sections. Note that the thickness of the manubrium (which is much thicker than the membrane) was not measured, causing a gap in the data for slices 0 and 3, respectively. The TM thickness is not uniform in any of these slices but follows either a W-shaped or a U-shaped profile. That is, the membrane is thicker near the outer edges as well as in those regions where the umbo/manubrium is attached, ~22–45 μm. This is consistent with the micrographs in the literature that the fiber layers appear thicker near the manubrium, umbo and peripheral rim resulting in thicker regions of the TM [e.g., cat, guinea pig: (Lim, 1968); gerbil: (Henson et al., 2005; von Unge et al., 1991)] Also, the TM thickness shows a gradual increase from inferior (slice −4) to umbo location (slide 0) to superior (slice 3) locations within the range of 9–23, 9–26, and 10–35 μm, respectively. Finally, the anterior side tends to be slightly thinner than the posterior side in the TM region superior to the umbo; inferior to the umbo, no anterior-posterior differences were observed. These trends are not limited to these three slices but are observed across the entire TM (Fig.2C).

The distribution of the thickness of each TM was reconstructed from linear interpolation of multiple-point measurements along the 11 cross-sections and two of them are shown in Fig. 2C. In general, for the normal TMs, in the region inferior to the umbo, the thickness reading is smallest and rather constant in the center, which increases when approaching the edge in a range of 9–20 μm. In the region superior to the umbo, the thickness distribution is approximately symmetrical anterior and posterior to the manubrium, ~ 15 μm, with thicker readings, ~30 μm, close to the manubrium and the annulus. One thing to note is that the very top and very bottom of the TM were not included in the measurement, thus, the shape of the TM in our thickness maps falsely portrays a rounder shape when compared to the actual more ovular shape of the TM.

3.2 The Thickness of Spontaneously Healed Tympanic Membranes under Fresh Condition

Visually, the spontaneously healed TM had a “rougher” and less uniform appearance than the control ears. The thickness measurements for the freshly imaged, spontaneously healed

TM are shown in Figure 3. These data are from six of eight animals; in two specimens the TM was fused to the tympanic ring in the healed areas, and their thickness measurements were excluded from further analysis. Although the thickness profiles are similarly W- or U-shaped, the overall thickness increased. This increase was most pronounced in the damaged area (slice −4), where TM thickness had doubled with a mean thickness of 30–40 μm, but was even present in TM regions that were not damaged by the initial perforation (e.g. slices 0 and 3 with thickness of was ~16–43 and 25–30 μm, respectively). This can also be appreciated by comparing the thickness maps from Figures 2C and 3C. Pars tensa of the spontaneously healed TM is markedly thicker, but this thickened area expands to non-damaged TM regions, consistent with observations at the cellular levels (Johnson et al., 1990).

3.3 Thickness Differences Between Fresh and Fixed Conditions

After scanning under fresh conditions, six normal and five spontaneously healed TMs were placed in a 4% paraformaldehyde fixative solution for 24 hours. The fixed TMs were then re-scanned with the OCT system and thickness measurements were repeated. These thickness measurements are presented in Fig. 4 by comparing earlier measurements of the same TMs under fresh (pre-fixing) conditions. Thus the average number of TMs was different from those in Fig. 3. A pairwise comparison (fresh vs. fixed) showed an average difference of less than 4 mm at all locations along each of the three representative slices, both for normal and spontaneously healed conditions. This difference is within the resolution (4.54 μm) of the system, indicating that the fixation process did not affect TM thickness. However, our results show a much thicker TM compared to published data from the same area of fresh gerbil TMs [pink regions in Fig. 4, which are from Fig. 3 in (Kuypers et al., 2005b)]. The difference might be from the different imaging methodology, which is further discussed in Discussion section.

3.4 Hearing and Middle Ear Transmission in Animals with Spontaneously Healed TMs

Hearing of the animals was monitored pre-perforation (normal condition) and weekly following the 50%-TM perforation using ABR thresholds. For gerbils with normal intact TMs, the ABR thresholds were around 10 dB SPL at 2–22 kHz (black line in Fig. 5A), with higher thresholds at lower and higher frequencies. These data are consistent with previous measures of gerbil hearing (Mason, 2016). The ABR thresholds elevated ~30 dB at all frequencies post perforation (dotted blue line in Fig. 5A) and recovered dramatically at frequencies below 20 kHz at week 2 (green line in Fig. 5A), a time at which the perforation was completely sealed. The ABR thresholds continued to recover over the healing process and were almost back to normal level at frequencies below 16 kHz at week 4 (red line in Fig. 5A). The ABR thresholds remained elevated at higher frequencies, i.e., > 20 kHz, and appeared to be stable even up to 8 weeks post-perforation.

To understand this hearing loss in gerbils with 50% perforated or healed TMs, MEPG, amplitude and phase responses were directly measured. The MEPG of gerbils with normal TM was ~20 dB and almost flat with frequency (black line in Fig. 5B), consistent with results published in the literature [i.e., (Dong et al., 2006)]. The slight roll-off in MEPG at

frequencies less than 1 kHz was due to the non-perfect sealing of the sound system to the ear canal (de La Rochefoucauld et al., 2010).

Compared to the averaged normal TM conditions, the MEPG reduced 20–40 dB post 50% perforation across frequencies (blue dotted in Fig. 5B), consistent with the increased ABR thresholds. After 4 weeks of recovery, the MEPG was back to normal for frequencies between 2 to 8 kHz (red lines in Fig. 5B). However, at lower (< 2 kHz) and higher frequencies (> 8 kHz), the healed MEPG did not fully recover. At frequencies of < 2 kHz and ~8–25 kHz, the recovered MEPG only deviated by ~5–10 dB from normal, while a decrease of up to 30–40 dB was present at frequencies above 35 kHz. Again, this pattern of loss roughly followed the pattern that was seen in ABRs of the spontaneously healed animals. The similarity between the (changes in) ABR thresholds and MEGPs is more easily seen in Fig. 5D, in which the relative values (re. normal TM) for these two metrics are directly compared. That is, a change in ABR thresholds is mimicked by a change in MEPG (compare solid vs. dashed lines). The non-exact match between the two metrics is at least partially explained by the reduced frequency and intensity resolution used in the determination of the ABR thresholds. This close correspondence also means that the changes in ABR threshold (re. normal) can be used to assess how the sound transmission through the ME is affected by the TM pathology. Finally, the phase of the MEPG (Fig 5C) indicate that the ME sound-transmission time, evaluated by the phase group delay, $\tau = -\Delta\varphi/\Delta f$, appeared to be longer in ears with healed TM (Fig. 5C), but was (nearly) normal in ears with 50% TM perforations.

4. DISCUSSION

The structure and physical properties of the TM are important for transmitting sounds to the ossicular chain, and any variations from normal TM conditions likely alter the auditory function, resulting in a CHL (Merchant et al., 2003a). TM perforation in patients, which tend to heal spontaneously, is commonly caused by either trauma or infection,. However, the healed TMs were found to be thicker and abnormally dense with elevated hearing thresholds (Cho et al., 2013; Garth, 1994). In cases that the TM perforation does not heal spontaneously, surgery is performed (tympanoplasty) to reconstruct the TM using material such as muscle fascia, perichondrium, and cartilage. Clinical observations indicate that the surgical techniques used to repair a perforated TM can lead to some restoration of the CHL postoperatively (Merchant et al., 2003a; Merchant et al., 2003b). However, in up to 30% of patients, there remains an abnormal residual air/bone gap that may vary from 5 to 35 dB (Puria et al., 2013), which continues to produce hearing difficulties.

In our study, we focused on ME sound transmission following the spontaneous recovery of a perforated pars tensa. The thickness distributions of gerbil TMs were mapped using a commercial OCT system. In addition, ME transmission (in terms of MEPG) and ABR thresholds of these ears were measured *in vivo*. We found that, although the TM heals (=closes) spontaneously after perforation, it remains much thicker throughout and normal hearing is not restored: there remains a substantial, high-frequency hearing loss that can be attributed to a less efficient sound transmission through the middle ear (Fig. 5). Also, the sound transmission time through the ME appeared to be longer. This is the first time that the

correlation between TM thickness and hearing function has been shown in the same gerbils. In addition, TM thickness distribution maps will be extremely valuable in refining models of TM function, especially under pathological conditions.

4.1 Determination of the examination time point at four weeks post-perforation:

Otoscopy was used to track the healing process of the TM over time, which allowed us to ensure that the TMs remained free of infection or excessive wax build up. Characterization of the healing process is described in detail in a recent publication (Dong et al., 2019). In general, following a 50%-perforation of the pars tensa, the gerbil TM began to close quickly, and after one week only ~10% of the perforation remained. The hole in the TM was completely sealed by week 2, which is a similar timeline as previously described for other laboratory rodents (Johnson et al., 1987; Johnson et al., 1990; Rahman et al., 2005; Stenfors et al., 1980; Wang et al., 2004). As examined with an otoscope, little change occurred as the time course continued after the fourth week, except for a slightly lesser extent of the thicker-looking opaque tissue on the healed membrane. In addition, ABR thresholds were used to evaluate hearing/functional restoration over the recovery period. By week 4, low-frequency ABR thresholds had returned to almost normal levels (Fig. 5A) at frequencies below 16 kHz. However, there was still ~20 dB threshold elevation at frequencies above 16 kHz, and this elevation of ABR thresholds remained little change up to 8 weeks. These observations made us use 4-weeks post-perforation as the terminal measurement point.

4.2 Advantages of using OCT system for thickness measurements:

OCT is a revolutionary imaging system that has been adapted to hearing research quickly. It provides more information that is not available for the classical essential visualization tools used by an otolaryngologist. For example, the otoscope and surgical microscope provide only surface imaging within a limited viewing angle, and without micro-scale features. OCT is a noninvasive, noncontact, rapid imaging system. It allows surface/3D visualization of tissue microstructure at high resolution in real time [Fig. 1 and reviews of (Ramier et al., 2018; Tan et al., 2018)], and has been used to characterize the thickness of TM in human temporal bones, in human subjects with normal TMs as well as in otitis media patient with abnormal TMs (Cho et al., 2015; Dsouza et al., 2018; Hubler et al., 2015; Park et al., 2018; Van der Jeught et al., 2013). In our study, we have demonstrated that a commercially available system can be used to map gerbil TM thickness distribution in a more efficient way compared to other conventional methods (e.g. histology). TM thickness measurements were obtained by taking a 3D scan of an entire TM within several seconds. The 3D scanning image was then easily sliced into many 2D cross-section images of the TM using the function of “B-Scans” (Fig. 1), and TM thickness measurements were then performed at each cross-section with a resolution of 3–5 μm. Our results confirm the potential application of OCT in both the clinic and in research laboratories as a diagnostic aid for otologic conditions.

4.3 TM thickness distribution under intact condition:

In a normal gerbil TM, we found the TM thickness is not uniform. The central portion of the gerbil pars tensa between the annulus and the manubrium was the thinnest, ~13–16 μm on average. The thickness increased close to the bone edge, ~20–30 μm in general (Figs. 2 and

4), resulting in a W- or U-shaped thickness pattern, like the one seen by Kuypers et al. (Kuypers et al., 2005a). The thickness measured in our study, however, appeared to be thicker than theirs at similar locations as our example slices (see Fig. 4). The difference here might be from the preparations of the TMs. In our study, the TMs were scanned within 30 min post mortem without any further processing, referred to as the "fresh" condition, and again 24 hours after fixation ("fixed" condition). We found no difference in the thickness estimates between these two methods (Fig. 4). In Kuypers's study, the TMs were stained by soaking for 30 min in water-based Van Giesson dye, which they claim does not cause dehydration or shrinking (Kuypers et al., 2005a; Kuypers et al., 2005b). If not the fixing process, the difference may arise from the mounting of the TMs. They mounted the TMs on a standard cover glass with their medial sides downwards, facing the objective lens. Limited by the working distance of their confocal lens (230 μm), the membranes had to be flattened, from their natural cone shape, across the glass. Although TM folds were avoided in the regions that had been measured, it is not clear whether these manipulations decreased the thickness of the membranes.

Other groups have measured the thicknesses of the gerbil TM. However, the majority of these studies used histological sectioning. It is not clear if, and to what extent, the histological preparation techniques affect the TM thickness. Using histological approaches, the gerbil TM was found to be anywhere from 3–20 μm in general (Teoh et al., 1997; von Unge et al., 1991; von Unge et al., 1999). Our study narrowed the range down to ~13–16 μm in the central region between the manubrium and annulus, and ~20–30 μm along the annular edge.

4.4 TM thickness distribution after spontaneously healing:

As the perforation starts to heal, the edges and the areas just past the edges start to thicken and advance to close the hole in a non-symmetrical way, following by a migration of spurs of epithelial cells towards the defects (Johnson et al., 1990). Granulation tissue progressively invades the area with abundant collagen fibers. A "leading edge" forms that looks both rough and jagged and migrates to close the perforation. Even after complete closure of the perforation, the thickness of both the healed areas and the areas near the perforation are non-uniform and thicker than normal (Johnson et al., 1990; Rahman et al., 2005; Stenfors et al., 1980). Thus, TMs display a thickened membrane not only over the healed-perforation locus, but also on areas adjacent to the perforation (Rahman et al., 2007; Rahman et al., 2005). As described in details in an earlier report (Dong et al., 2019), by week-4 the gerbil TM-50%-perforation appeared to be completely healed and some of the visible scar tissue was starting to be reduced. However, the thickness measurements of the healed TM revealed a much thicker pars tensa than a normal TM, especially around the perforation area. Also, the thickness was not homogenous across the healed area (Figs. 3 & 4). The central portion of the TM between the annulus and manubrium measured anywhere from 25–65 μm, with the edges again slightly thicker. Our results are consistent with reports in the literature, e.g., two-weeks post-perforation, rat TM appear to be 5 times thicker than normal (Rahman et al., 2005) and even after 10 weeks, or half a year, the healed perforation area was clearly thicker in cats and rats (Rahman et al., 2007; Stenfors et al., 1980). The thicker TM was due to the irregular structure exhibited in these animals, i.e., ingrowth of fibroblasts and extracellular

matrix with fiber-like structures without an obvious system of orientation (Henson et al., 2005; Lim, 1968; von Unge et al., 1991). Thus, the thickness measurements help to confirm the deviations from normal in functional evaluations in the healing process.

4.5 The role of TM in sound transmission and clinical significance:

Variations in the physical properties of the TM directly influence sound transmission through the ME. For spontaneously healed TMs, the variations include increased thickness and amount of fibers exhibited with an obvious lacking of the reorganization of the fiber layer. These structural changes suggest a variation in stiffness and increased mass of the healed TM, properties that will affect the mechanical responses of this membrane.

Effects of mechanical properties of the TM on ME sound transmission has been detailed described in theoretical models, i.e., 3D finite-element (FE) models (Caminos et al., 2018; O'Connor et al., 2017). The mass of the TM was found to have little effect on the MEPG at low frequencies [Fig. 3 in (O'Connor et al., 2017)]; however, it showed an inverse relationship to the MEPG at mid-to-high frequencies. According to the 3D FE model prediction, a 5–10× increase in mass caused reduction in the MEPG amplitude up to 20 dB in the mid- and high-frequency region. In addition, increased mass led to up to 2xlonger ME transmission times. In their model, the influence of TM fiber distribution/stiffness in radial, circumferential, and transverse direction was also discussed. Their results depend on several model restrictions, e.g., isotropic vs orthotropic TM, "soft" vs "hard" boundary conditions, variation in shear vs Young's modulus, but indicate that variation in the stiffness of radial collagen fibers has the largest effect on the MEPG, especially at high frequencies. These predictions are consistent with measurements from human cadaveric temporal bones in that radial distributed fibers played greater role in ME sound transmission at frequencies above 4 kHz than circumferential arranged fibers (O'Connor et al., 2008). In another 3D FE prediction, effects of TM thickness were discussed (Caminos et al., 2018). Here, an increased TM thickness was considered to increase both the mass and stiffness. Model results showed an overall reduction pattern across frequencies in the ME transmission but more so in the low frequency region.

In the current study, the ME transmission evaluated by ABR and directly measured using MEPG in ears with healed TMs appeared to be back to normal at frequencies below 8 kHz, less efficient (< 10 dB loss) at low- (< 2 kHz) and mid-frequencies (8–25 kHz) and 20 dB or more loss at higher frequencies (Fig. 5). These results are consistent with findings in patients with spontaneously healed TM perforations who experienced blast injuries during the Boston Marathon on April 15, 2013 (Remenschneider et al., 2014). In addition, we found that the delay of ME sound transmission (evaluated by the phase group delay) appeared to be longer after TM healing. According to the model predictions discussed above, the variations in the ME transmission (amplitude and phase) we observed in these healed ears appeared to result from the combined effects of an increased mass and a non-organized fiber distribution.

Our results also offer some explanations for the outcomes following tympanoplasty. This procedure re-establishes the barrier between the ear canal and ME when a TM perforation does not heal spontaneously. For the reconstruction, muscle fascia and cartilage are routinely used (Mouna et al. 2019). The cartilage plate is normally prepared with a thickness of ~500

μm [i.e., (Beutner et al., 2010)]; significantly thicker than a normal human TM (50–120μ m) (Hubler et al., 2015; Van der Jeught et al., 2013). And the temporalis fascia was demonstrated not significantly remodel, change thickness or change fiber structure following successful tympanoplasty (Trakimas et al., 2018); its thickness was about 2× that of the normal TM, sixteen years post operation.. The reconstructed, and thickened, TM effectively restored low-frequency hearing, but did little to recover hearing at high frequencies. Thus, as suggested by our results, the mechanical properties of the TM are important to sound transmission, especially at the high-frequency region. To improve hearing following tympanoplasty it seems pertinent to mimic the structural properties of the TM, rather than simply “closing the gap”, perhaps using advances in 3D printing and stem cell techniques (Kozin et al., 2016).

In summary: Mapping the TM thickness is valuable in understanding the ME sound transmission under normal and pathological conditions. We used a gerbil model with a spontaneously healed TM following a 4-week recovery post-perforation of pars tensa to map the TM thickness using a high-resolution commercial OCT imaging system. The system allowed us to reconstruct the TM thickness distribution in an efficient way. The normal TMs were not perfectly homogeneous, with the thinner reading of ~13–16 μm in average in the central portion of the pars tensa, and gradually increased thickness while approaching the annulus, ~20–30 μm thick in general. The healed TMs showed rough surface, displayed thickened membrane, ~2–3 times to the normal, not only over the healed-perforation locus, but also on areas adjacent to the perforation. The thickness distribution demonstrated the variation of physical properties in the healed TM leading to non-recovered ME sound transmission, especially at high frequencies, which is consistent with model predictions.

Acknowledgments:

The authors would like to thank Justin Li and Brandon Shin to work out the method of using OCT scanning to perform TM thickness measurements. And thanks to Sebastiaan W. F. Meenderink for the helpful comments, discussions, and modification on the manuscript.

Funding:

The research work was performed at facilities provided by the Department of Veterans Affairs. This study was supported by VA Merit Award C2296-R (Dong), NIDCD R01DC011506 (Dong), and the Department of Otolaryngology Head & Neck Surgery, at Loma Linda University Health. These contents do not represent the views of the U.S. Department of Veterans Affairs or the United States Government.

Abbreviations:

3D	three-dimensional
ABR	auditory brainstem response
CHL	conductive hearing loss
dB	decibel
DPOAE	distortion product otoacoustic emission
IACUC	the Institutional Animal Care and Use Committee

ME	middle ear
MEPG	middle ear pressure gain
OCT	optical coherence tomography
P_{TM}	pressure at the tympanic membrane near the umbo
P_{SV}	pressure in the scala vestibuli near the stapes
SPL	sound pressure levels
SV	scala vestibuli
TM	tympanic membrane

References:

Beutner D, Huttenbrink KB, Stumpf R, Beleites T, Zahnert T, Luers JC, Helmstaedter V 2010 Cartilage plate tympanoplasty. Otol Neurotol 31, 105–10. [PubMed: 19816225]

Caminos L, Garcia-Manrique J, Lima-Rodriguez A, Gonzalez-Herrera A 2018 Analysis of the Mechanical Properties of the Human Tympanic Membrane and Its Influence on the Dynamic Behaviour of the Human Hearing System. Appl Bionics Biomech 2018, 1736957. [PubMed: 29853992]

Cheng JT, Hamade M, Merchant SN, Rosowski JJ, Harrington E, Furlong C 2013 Wave motion on the surface of the human tympanic membrane: holographic measurement and modeling analysis. The Journal of the Acoustical Society of America 133, 918–37. [PubMed: 23363110]

Cheng JT, Aarnisalo AA, Harrington E, Hernandez-Montes Mdel S, Furlong C, Merchant SN, Rosowski JJ 2010 Motion of the surface of the human tympanic membrane measured with stroboscopic holography. Hearing research 263, 66–77. [PubMed: 20034549]

Cho NH, Lee SH, Jung W, Jang JH, Kim J 2015 Optical coherence tomography for the diagnosis and evaluation of human otitis media. J Korean Med Sci 30, 328–35. [PubMed: 25729258]

Cho SI, Gao SS, Xia A, Wang R, Salles FT, Raphael PD, Abaya H, Wachtel J, Baek J, Jacobs D, Rasband MN, Oghalai JS 2013 Mechanisms of hearing loss after blast injury to the ear. PLoS One 8, e67618. [PubMed: 23840874]

de La Rochefoucauld O, Kachroo P, Olson ES 2010 Ossicular motion related to middle ear transmission delay in gerbil. Hearing research 270, 158–72. [PubMed: 20696229]

Decraemer WF, Funnell WR 2008 Anatomical and mechanical properties of the tympanic membrane, Chronic otitis media Pathogenesis-oriented theropeutic management. Kugler Publications, The Hague, Amsterdam, The Netherlands pp. 51–84.

Djalilian HR, Ridgway J, Tam M, Sepehr A, Chen Z, Wong BJ 2008 Imaging the human tympanic membrane using optical coherence tomography in vivo. Otol Neurotol 29, 1091–4. [PubMed: 18957904]

Dong W, Olson ES 2006 Middle ear forward and reverse transmission in gerbil. Journal of neurophysiology 95, 2951–61. [PubMed: 16481455]

Dong W, Varavva P, Olson ES 2013 Sound transmission along the ossicular chain in common wild-type laboratory mice. Hearing research 301, 27–34. [PubMed: 23183032]

Dong W, Stomackin G, Lin X, Martin GK, Jung TT 2019 Distortion product otoacoustic emissions: Sensitive measures of tympanic -membrane perforation and healing processes in a gerbil model. Hearing research.

Dsouza R, Won J, Monroy GL, Hill MC, Porter RG, Novak MA, Boppart SA 2018 In vivo detection of nanometer-scale structural changes of the human tympanic membrane in otitis media. Sci Rep 8, 8777. [PubMed: 29884809]

Garth RJ 1994 Blast injury of the auditory system: a review of the mechanisms and pathology. The Journal of laryngology and otology 108, 925–9. [PubMed: 7829942]

Heffner HE, Heffner RS 2007 Hearing ranges of laboratory animals. J Am Assoc Lab Anim Sci 46, 20–2.

Henson MM, Madden VJ, Rask-Andersen H, Henson OW Jr. 2005 Smooth muscle in the annulus fibrosus of the tympanic membrane in bats, rodents, insectivores, and humans. Hearing research 200, 29–37. [PubMed: 15668036]

Huang D, Swanson EA, Lin CP, Schuman JS, Stinson WG, Chang W, Hee MR, Flotte T, Gregory K, Puliafito CA, et al. 1991 Optical coherence tomography. Science 254, 1178–81. [PubMed: 1957169]

Hubler Z, Shemonski ND, Shelton RL, Monroy GL, Nolan RM, Boppart SA 2015 Real-time automated thickness measurement of the in vivo human tympanic membrane using optical coherence tomography. Quant Imaging Med Surg 5, 69–77. [PubMed: 25694956]

Johnson A, Hawke M 1987 The function of migratory epidermis in the healing of tympanic membrane perforations in guinea-pig. A photographic study. Acta oto-laryngologica 103, 81–6. [PubMed: 3564931]

Johnson AP, Smallman LA, Kent SE 1990 The mechanism of healing of tympanic membrane perforations. A two-dimensional histological study in guinea pigs. Acta oto-laryngologica 109, 406–15. [PubMed: 2360447]

Khanna SM, Tonndorf J 1972 Tympanic membrane vibrations in cats studied by time-averaged holography. The Journal of the Acoustical Society of America 51, 1904–20. [PubMed: 5045250]

Kozin ED, Black NL, Cheng JT, Cotler MJ, McKenna MJ, Lee DJ, Lewis JA, Rosowski JJ, Remenschneider AK 2016 Design, fabrication, and in vitro testing of novel three-dimensionally printed tympanic membrane grafts. Hearing research 340, 191–203. [PubMed: 26994661]

Kuypers LC, Decraemer WF, Dirckx JJ, Timmermans JP 2005a Thickness distribution of fresh eardrums of cat obtained with confocal microscopy. Journal of the Association for Research in Otolaryngology : JARO 6, 223–33. [PubMed: 15983727]

Kuypers LC, Dirckx JJ, Decraemer WF, Timmermans JP 2005b Thickness of the gerbil tympanic membrane measured with confocal microscopy. Hearing research 209, 42–52. [PubMed: 16054789]

Lim DJ 1968 Tympanic membrane. Electron microscopic observation. I: pars tensa. Acta oto-laryngologica 66, 181–98. [PubMed: 4974041]

Lim DJ 1970 Human tympanic membrane. An ultrastructural observation. Acta oto-laryngologica 70, 176–86. [PubMed: 5477148]

Mason MJ 2016 Structure and function of the mammalian middle ear. II: Inferring function from structure. Journal of Anatomy 228, 300–12. [PubMed: 26100915]

Merchant SN, Rosowski JJ, McKenna MJ 2003a Tympanoplasty. Operative Techiniques in Otolaryngology-Head and Neck Surgery 14, 224–236.

Merchant SN, McKenna MJ, Mehta RP, Ravicz ME, Rosowski JJ 2003b Middle ear mechanics of Type III tympanoplasty (stapes columella): II. Clinical studies. Otol Neurotol 24, 186–94. [PubMed: 12621330]

Monroy GL, Shelton RL, Nolan RM, Nguyen CT, Novak MA, Hill MC, McCormick DT, Boppart SA 2015 Noninvasive depth-resolved optical measurements of the tympanic membrane and middle ear for differentiating otitis media. The Laryngoscope 125, E276–82. [PubMed: 25599652]

Nguyen CT, Jung W, Kim J, Chaney EJ, Novak M, Stewart CN, Boppart SA 2012 Noninvasive in vivo optical detection of biofilm in the human middle ear. Proc Natl Acad Sci U S A 109, 9529–34. [PubMed: 22645342]

O'Connor KN, Cai H, Puria S 2017 The effects of varying tympanic-membrane material properties on human middle-ear sound transmission in a three-dimensional finite-element model. The Journal of the Acoustical Society of America 142, 2836. [PubMed: 29195482]

O'Connor KN, Tam M, Blevins NH, Puria S 2008 Tympanic membrane collagen fibers: a key to high-frequency sound conduction. The Laryngoscope 118, 483–90. [PubMed: 18091335]

Olson ES 1998 Observing middle and inner ear mechanics with novel intracochlear pressure sensors. The Journal of the Acoustical Society of America 103, 3445–63. [PubMed: 9637031]

Olson ES, Nakajima HH 2015 A family of fiber-optic based pressure sensors for intracochlear measurements. SPIE BIOS.

Park K, Cho NH, Jeon M, Lee SH, Jang JH, Boppart SA, Jung W, Kim J 2018 Optical assessment of the in vivo tympanic membrane status using a handheld optical coherence tomography-based otoscope. Acta oto-laryngologica 138, 367–374. [PubMed: 29125012]

Pitris C, Saunders KT, Fujimoto JG, Brezinski ME 2001 High-resolution imaging of the middle ear with optical coherence tomography: a feasibility study. Arch Otolaryngol Head Neck Surg 127, 637–42. [PubMed: 11405861]

Puria S, Fay RR, Popper A 2013 The Middle Ear, Springer Handbook of Auditory Research, Vol. 46, 1 ed. Springer-Verlag New York. pp. 1–308.

Rahman A, Hultcrantz M, Dirckx J, von Unge M 2007 Structural and functional properties of the healed tympanic membrane: a long-term follow-up after laser myringotomy. Otol Neurotol 28, 685–91. [PubMed: 17429337]

Rahman A, Hultcrantz M, Dirckx J, Margolin G, von Unge M 2005 Fresh tympanic membrane perforations heal without significant loss of strength. Otol Neurotol 26, 1100–6. [PubMed: 16272923]

Ramier A, Cheng JT, Ravicz ME, Rosowski JJ, Yun SH 2018 Mapping the phase and amplitude of ossicular chain motion using sound-synchronous optical coherence vibrography. Biomed Opt Express 9, 5489–5502. [PubMed: 30460142]

Remenschneider AK, Lookabaugh S, Aliphas A, Brodsky JR, Devaiah AK, Dagher W, Grundfast KM, Heman-Ackah SE, Rubin S, Sillman J, Tsai AC, Vecchiotti M, Kujawa SG, Lee DJ, Quesnel AM 2014 Otologic outcomes after blast injury: the Boston Marathon experience. Otol Neurotol 35, 1825–34. [PubMed: 25393974]

Rosowski JJ, Cheng JT, Ravicz ME, Hulli N, Hernandez-Montes M, Harrington E, Furlong C 2009 Computer-assisted time-averaged holograms of the motion of the surface of the mammalian tympanic membrane with sound stimuli of 0.4–25 kHz. Hearing research 253, 83–96. [PubMed: 19328841]

Ryan A 1976 Hearing sensitivity of the mongolian gerbil, Meriones unguiculatis. The Journal of the Acoustical Society of America 59, 1222–6. [PubMed: 956517]

Shelton RL, Jung W, Sayegh SI, McCormick DT, Kim J, Boppart SA 2014 Optical coherence tomography for advanced screening in the primary care office. J Biophotonics 7, 525–33. [PubMed: 23606343]

Stenfors LE, Carlsoo B, Salen B, Winblad B 1980 Repair of experimental tympanic membrane perforations. Acta oto-laryngologica 90, 332–41. [PubMed: 7211327]

Stomackin G, Kidd S, Jung TT, Martin GK, Dong W 2018 Effects of tympanic membrane perforation on middle ear transmission in gerbil. Hearing research 373, 48–58. [PubMed: 30583199]

Stomackin G, Kidd S, Jung TT, Martin GK, Dong W 2019 Effects of tympanic membrane perforation on middle ear transmission in gerbil. Hearing research 373, 48–58. [PubMed: 30583199]

Tan HEI, Santa Maria PL, Wijesinghe P, Francis Kennedy B, Allardyce BJ, Eikelboom RH, Atlas MD, Dilley RJ 2018 Optical Coherence Tomography of the Tympanic Membrane and Middle Ear: A Review. Otolaryngol Head Neck Surg 159, 424–438. [PubMed: 29787354]

Teoh SW, Flandermeyer DT, Rosowski JJ 1997 Effects of pars flaccida on sound conduction in ears of Mongolian gerbil: acoustic and anatomical measurements. Hearing research 106, 39–65. [PubMed: 9112106]

Trakimas DR, Ishai R, Ghanad I, Black NL, Kozin ED, Cheng JT, Remenschneider AK 2018 Otopathologic evaluation of temporalis fascia grafts following successful tympanoplasty in humans. The Laryngoscope 128, E351–E358. [PubMed: 29756238]

Van der Jeught S, Dirckx JJ, Aerts JR, Bradu A, Podoleanu AG, Buytaert JA 2013 Full-field thickness distribution of human tympanic membrane obtained with optical coherence tomography. Journal of the Association for Research in Otolaryngology : JARO 14, 483–94. [PubMed: 23673509]

von Unge M, Bagger-Sjoback D, Borg E 1991 Mechanoacoustic properties of the tympanic membrane: a study on isolated Mongolian gerbil temporal bones. Am J Otol 12, 407–19. [PubMed: 1805631]

von Unge M, Decraemer WF, Dirckx JJ, Bagger-Sjoback D 1999 Tympanic membrane displacement patterns in experimental cholesteatoma. Hearing research 128, 1–15. [PubMed: 10082278]

Voss SE, Rosowski JJ, Merchant SN, Peake WT 2001 Middle-ear function with tympanic-membrane perforations. I. Measurements and mechanisms. The Journal of the Acoustical Society of America 110, 1432–44. [PubMed: 11572354]

Wang WQ, Wang ZM, Chi FL 2004 Spontaneous healing of various tympanic membrane perforations in the rat. Acta oto-laryngologica 124, 1141–4. [PubMed: 15768806]

- OCT is an efficient technology to quickly and noninvasively map TM thickness
- TM structural recovery leads to functional recovery
- Spontaneously healed TM are thicker than normal, which affects ME transmission
- After perforation, healed TM are functionally *not* normal, resulting in hearing loss
- Thickening of the inferior TM portion reduces high-frequency sound transmission

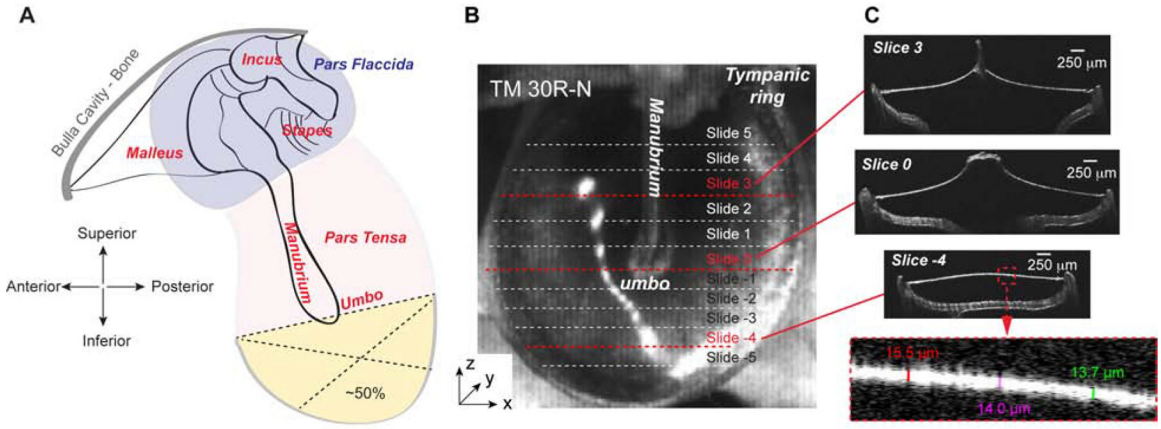

Figure 1. Diagram of TM perforation and thickness measurements using the OCT system.

(A) Diagram of TM perforation. The perforation was introduced at the inferior of the pars tensa to 50% (yellow area) using the umbo as the reference location. **(B)** 3D scanned OCT image of a normal TM (TM 30R-N). Dotted lines indicate cross sections along which the thickness was measured. **(C)** Cross-sectional OCT images of three representative locations as indicated by red dashed lines in panel B. These images were taken from locations above, at, and under the umbo, perpendicular to the manubrium. The bottom panel is the zoomed in portion of the Slice −4 to illustrate how the thickness of the TM was measured.

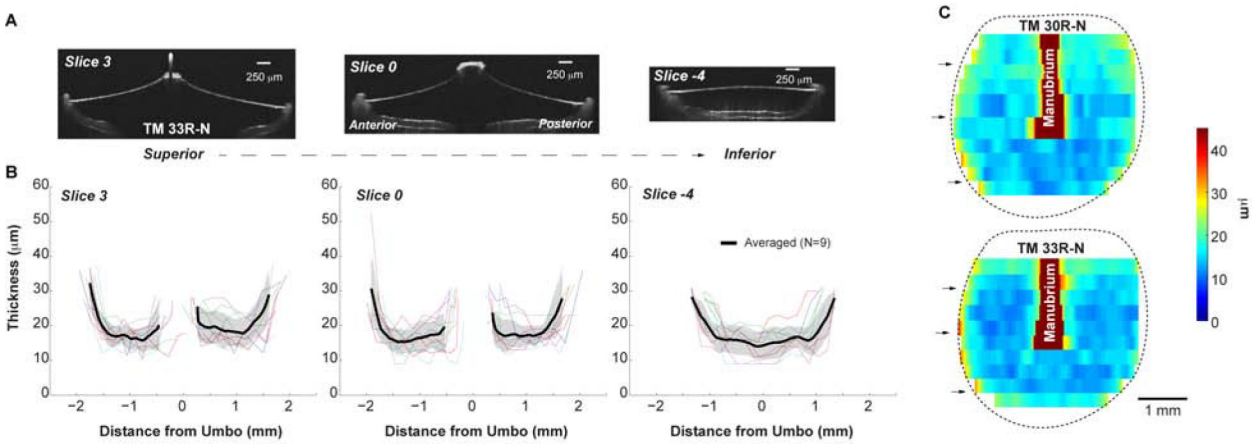

Figure 2. Thicknesses of fresh normal TMs.

(A) OCT images of three representative cross-sections of the TM (TM 33R-N, cross-sections of the other example, TM 30R-N, are in Fig. 1C); **(B)** Thickness reading of the corresponding cross-sections of normal TMs. Thin lines represent the thickness of each individual TM. Black line and shaded area stand for the Mean ± SD of 9 TMs. SD: standard deviation. **(C)** Distribution of the thickness maps of two normal TMs under fresh condition, reconstructed from linear interpretation of 11 cross section measurements. Black arrows indicate the locations of the representative slices shown in panel B. Dotted lines represent the boundary of the pars tensa.

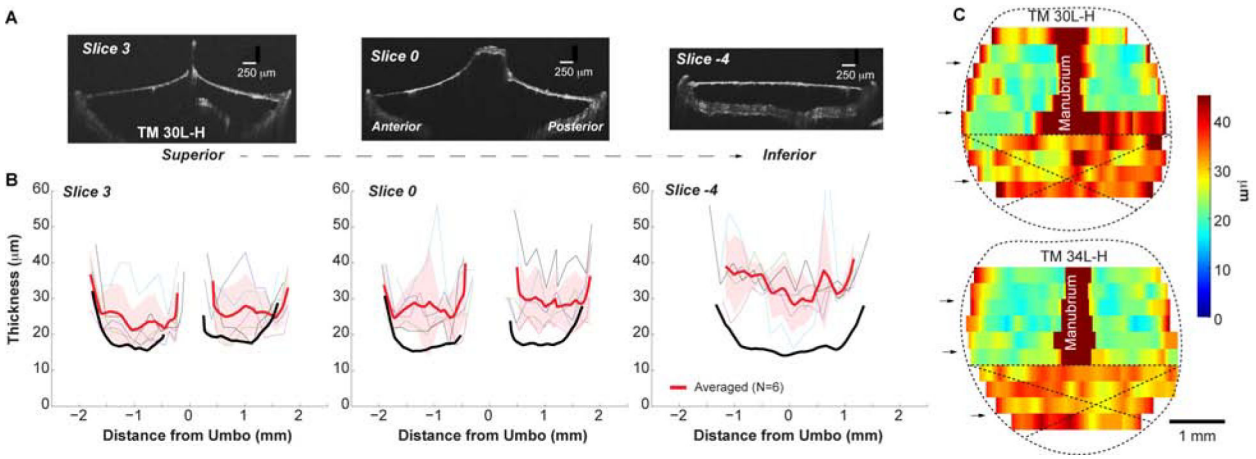

Figure 3. Thicknesses of fresh spontaneously healed TMs post-50%-perforation.

(A) OCT images under fresh conditions of the representative cross-sections of the post-50%-perforation spontaneously healed TM of animal # 30L-H; **(B)** Thickness reading of the corresponding cross-sections from individual (thin lines) and averaged TMs (thick red line). The thick red line and shaded area stand for the Mean ± SD of 6 TMs. As a comparison, the averaged thicknesses of the normal TMs at the same locations were plotted in black lines (same data as in Fig. 2B). **(C)** Distribution of the thickness maps of healed TMs post-50%-perforation under fresh condition. Black arrows indicate the locations of the representative slices shown in panel B. Crosses was used to indicate the original perforation area.

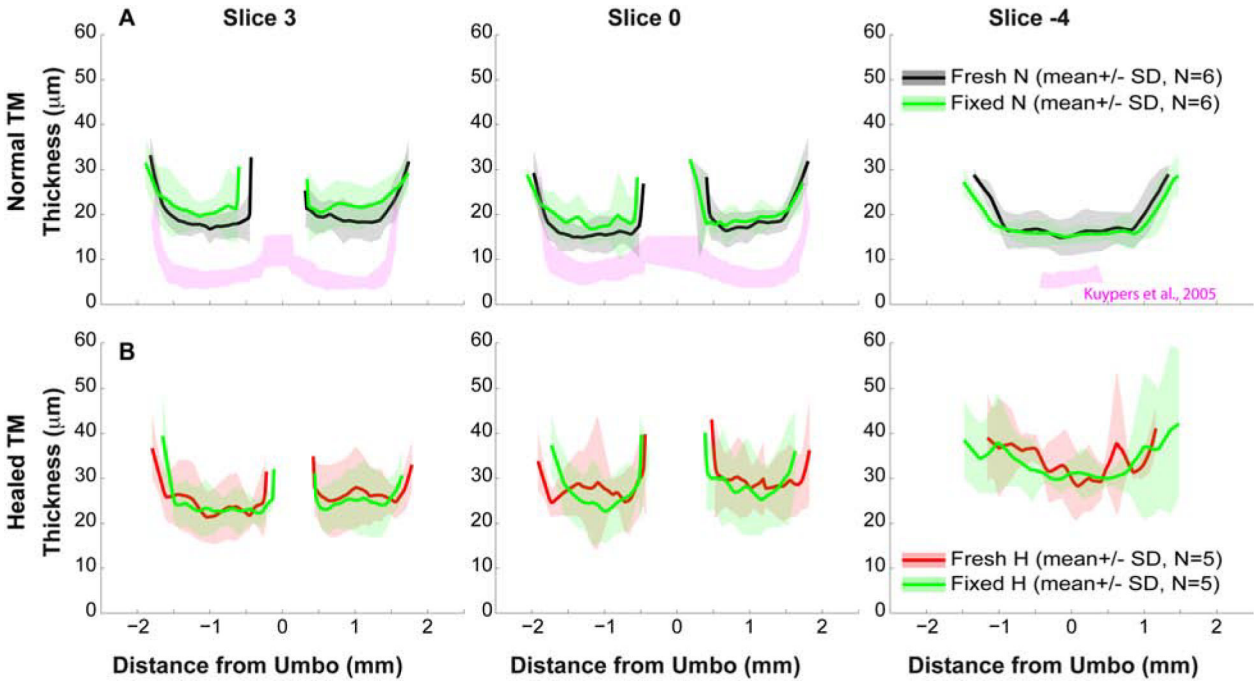

Figure 4. Comparisons of thickness of the same TM measured under fresh and fixed conditions.

Thickness of the three representative cross-sections of **(A)** normal and **(B)** healed TMs. Black, red and green lines along with shaded area represent Mean ± SD of normal and healed TMs under fresh and fixed conditions, respectively. For comparison, published data of thicknesses of normal gerbil TMs at the similar locations were also plotted in pink [Fig. 3 in (Kuypers et al., 2005b)].

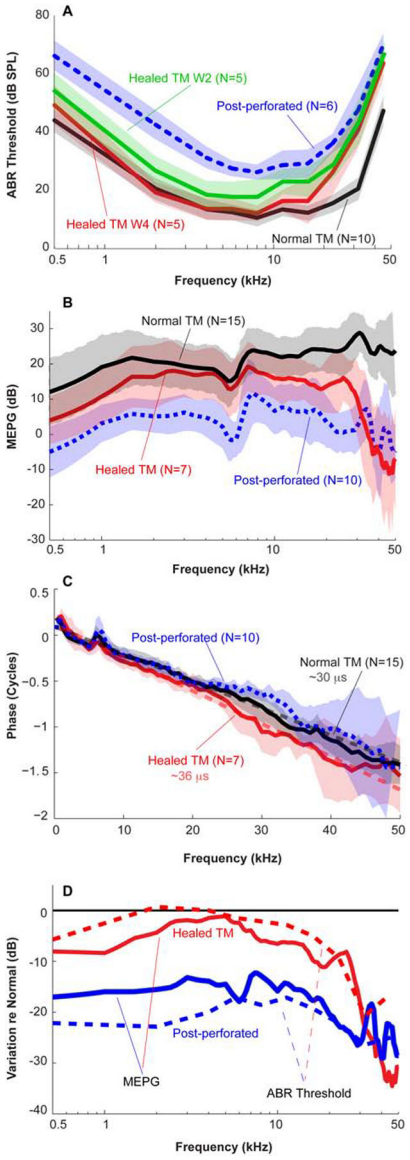

Figure 5. Hearing evaluation of animals with spontaneously healed TMs.

(A) ABR thresholds; **(B)** MEPG defined as $|P_{SV}|/|P_{TM}|$; **(C)** MEPG phase responses defined as $\phi P_{SV} - \phi P_{TM}$; **(D)** Changes in ABR threshold and MEPG relative to normal conditions. Solid and dashed lines stand for ABR threshold and MEPG, respectively. For comparison, mean±SD across animals with intact, immediate post-50%-perforation, post-perforation week 2 and week 4 defined as healed TMs were plotted as black, dotted-blue, green and red lines and shaded areas. Averaged data of post-perforation was from another group of animals for study of effects of size-dependent TM perforation on middle ear transmissions (Stomackin et al., 2018).